iScience

CellPress
OPEN ACCESS

Article

Topology optimization for near-junction thermal spreading of electronics in ballistic-diffusive regime

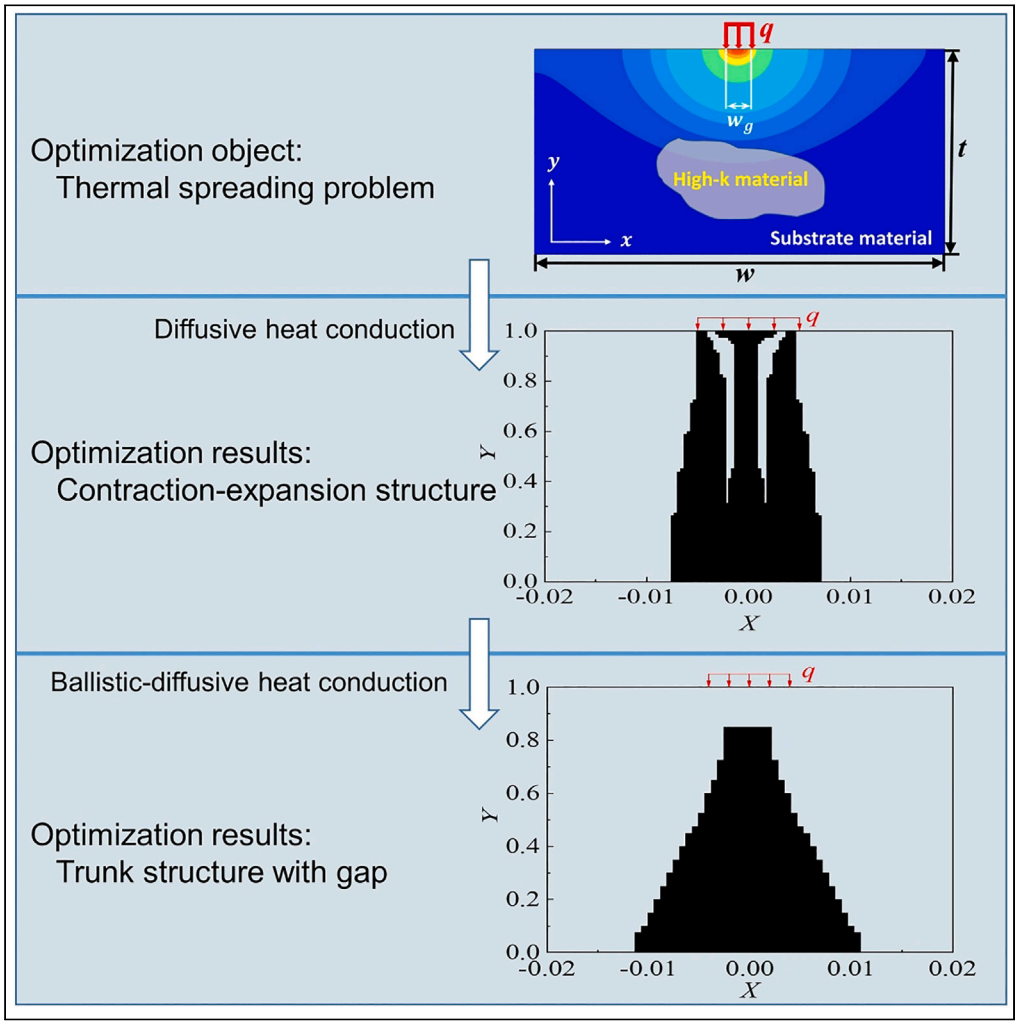

Zheng-Lai Tang, Yang Shen, Han-Ling Li, Bing-Yang Cao

caoby@tsinghua.edu.cn

Highlights

Developed a topology optimization method under ballistic-diffusive heat conduction

Contraction-expansion structure can reduce thermal resistance in thermal spreading

Results show phonon ballistic effects affect optimal material distributions

Tang et al., iScience 26, 107179
July 21, 2023
https://doi.org/10.1016/j.isci.2023.107179

iScience

CellPress
OPEN ACCESS

Article

Topology optimization for near-junction thermal spreading of electronics in ballistic-diffusive regime

Zheng-Lai Tang,[1] Yang Shen,[1] Han-Ling Li,[1] and Bing-Yang Cao[1,2,*]

SUMMARY

Hotspots in electronic devices can cause overheating and reduce performance. Enhancing the thermal spreading ability is critical for reducing device temperature to improve the reliability. However, as devices shrink, phonon ballistic effects can increase thermal resistance, making conventional optimization methods less effective. This paper presents a topology optimization method that combines the phonon Boltzmann transport equation with solid isotropic material with penalization method to optimize high thermal conductivity (HTC) material distributions for thermal spreading problems. Results show that the contraction-expansion structure can effectively reduce thermal resistance. Optimal distributions differ from that based on Fourier's heat conduction law, and only the trunk structure appears in optimized layouts due to the size effect. Additionally, HTC material with longer mean free paths tends to be filled around the heat source with a gap in a ballistic-diffusive regime. This work deepens understanding of thermal spreading and aids in thermal optimization of microelectronic chips.

INTRODUCTION

The high integration and miniaturization of chips lead to a continuous increase in the theoretical maximum power of chips, exemplified by Intel's latest chip exceeding 120 W.[1] However, this extremely high power density results in elevated chip temperatures, which can reduce reliability, performance, and lifespan. Therefore, it is crucial to develop efficient thermal management technologies to effectively dissipate heat from chips and address these challenges. Hotspots are a common issue in electronic devices due to non-uniform heat generation during chip operation.[2,3] Yet the self-heating effect in electronics, such as high electron mobility transistors (HEMTs), is mostly confined to a small region about 100 nm beneath the gate, whereas the channel and substrate layers have a total thickness in the hundreds of microns range.[4–6] It will cause a significant near-junction spreading resistance when heat is transferred from a small hotspot to a much larger region.[7,8] Furthermore, as device size decreases, the ballistic transport of phonons can further increase thermal spreading resistance, leading to higher hotspot temperatures.[9] Therefore, thermal optimization for the near-junction thermal spreading is crucial for the design and manufacture of advanced electronic devices for their reliable operations.[10]

One of the most useful methods to improve the heat dissipation capacity of thermal spreading is to use high thermal conductivity (HTC) materials, alike the volume-to-point problem.[11–13] One approach is to apply the nanofilm of HTC materials, such as diamond or graphene, to the top surface of the device.[14,15] Due to their ultra-HTC, with diamond having a thermal conductivity of approximately 400 W/m·K and graphene having a thermal conductivity of 1300–2800 W/m·K, these materials can effectively dissipate heat. As a result, incorporating 1–4 μm diamond or 4 nm graphene into the design of electronic devices can help to reduce the temperature of the device and improve its overall performance. Another option is to incorporate limited HTC materials into the electronics inside the device. The filled HTC materials can construct heat conduction pathways that efficiently extract heat from the hotspot thereby reducing the device temperature.[16] Due to the limited space within the chip, the amount of filled material must be restricted. Therefore, the optimization problem can be reduced to, finding HTC material distributions that reduce system temperature to a minimum value with a fixed filling rate. Many optimization methods have been developed for this type of material distribution optimization problem based on Fourier's heat conduction law, including constructal theory,[11] bionic optimization methods,[17–19] topology optimization,[20–22] simulated

[1]Key Laboratory of Thermal Science and Power Engineering of Education of Ministry, Department of Engineering Mechanics, Tsinghua University, Beijing 100084, China

[2]Lead contact

*Correspondence: caoby@tsinghua.edu.cn

https://doi.org/10.1016/j.isci.2023.107179

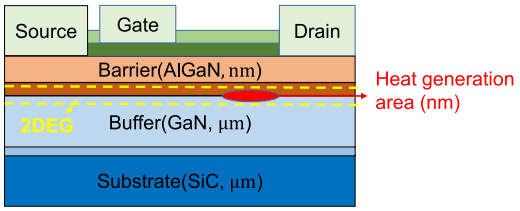

Figure 1. Typical structure of GaN HEMTs

annealing,[23] genetic algorithms,[24,25] etc. Among these methods, topology optimization is an increasingly attractive approach because it can change the topological configuration of the structure and has the highest degree of freedom in theory.[26]

Topology optimization is a mathematical method to optimize the material layout within a given design space.[26] The proposal of solid isotropic material with penalization (SIMP) facilitated the transition of design variable to the continuous which increased feasibility and generalizability.[27] Most of existing works of thermal topology optimization use Fourier's heat conduction law to describe the heat conduction process.[20–22] However, in semiconductors, the primary heat carriers are phonons, whose mean free paths can range from nanometers to several micrometers.[28] As the characteristic length of modern electronic devices reduces, the size of hotspots can be comparable or even smaller than the phonon mean free paths (MFPs).[29] In this regime, Fourier's heat conduction law becomes inapplicable, and ballistic-diffusive heat conduction emerges.[30–32] Phonon ballistic effects can significantly impact the heat transport mechanism and increase thermal resistance.[33–36] In this case, Fourier's heat conduction law-based optimizations may mislead thermal designs or even worsen heat dissipation. For typical semiconductor materials like gallium nitride (GaN), the phonon MFPs are generally much larger than 100 nm.[37] But in GaN HEMTs, the size of the hotspot is around 100 nm and the thickness of the buffer layer is between 1 and 3 μm, which results in a strong ballistic effect. Previous studies used dynamics theory and topology optimization to address non-Fourier's law thermal management issues, but their optimization goal was only to minimize temperature differences at specific points.[38] Therefore, it is necessary to develop the new optimization techniques that can account for non-Fourier, and thoroughly examine the influence of phonon ballistic effects on the thermal optimizations.

In this paper, we propose a new topology optimization method that couples the phonon Boltzmann transport equation (BTE) and SIMP for ballistic-diffusive heat conduction. Using the method, we conducted material distribution optimization for the thermal spreading problems, which is a representative hotspot system in electronic devices. The principle and mechanism of material filling in the thermal spreading process is analyzed and the influence of phonon ballistic effects is investigated thoroughly. This work can provide a more in-depth understanding of the thermal spreading process in a ballistic-diffusive regime and can be helpful for the thermal optimization of advanced electronic devices.

RESULTS

Basic structures of thermal spreading problem

The typical structure of GaN HEMTs, as shown in Figure 1, is a multi-layer thin film structure. It starts with a substrate made of silicon carbide, onto which a buffer layer made of GaN is grown. The thickness of the buffer layer is usually 1–3 μm. On top of the buffer layer, a barrier layer composed of AlGaN is grown, with a thickness of 10–30 nm.[6] Due to the polarization of the GaN and AlGaN heterojunction interface, a two-dimensional electron gas is generated at the interface. The main heat generation area during HEMT operation is the conductive channel, which has a thickness of several nanometers under the two-dimensional electron gas. The size of the hotspot is about 100 nm. However, the sum of the thickness of the buffer layer and the substrate is greater than 100 μm, which is much larger than the size of the heat source. It is important to note that optimizing heat dissipation in such HEMT structures can be challenging because it is difficult to strictly follow the fixed structure to fill HTC materials. However, backside via holes and other heat dissipation structures can improve the capability of devices.[39] In our study, we aim to derive more general physical laws by abstracting the thermal problem in HEMT structure and provide insights into future heat dissipation optimization.

The heat conduction process in GaN HEMTs is a typical thermal spreading process which can be abstracted to a 2D model as shown in Figure 2. The structure has a width denoted by w and a thickness denoted by t. At

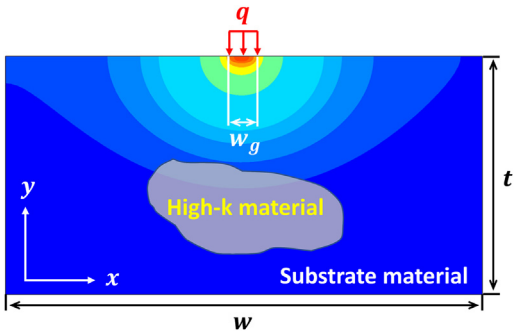

Figure 2. Schematic of the optimization of material distributions for thermal spreading process

the top of the system, there is a heat source with a small width of w_g and a heat flux density of q. The rest of the top boundary is adiabatic, and the lateral boundaries are all periodic. The lower boundary serves as an isothermal heat sink with $T = T_0$. In this study, w_g is set equal to $w/100$, and t/w is set as 40. This set of parameters ensures a strong ballistic effect and thermal spreading effect.[9] Initially, the system is full of substrate material with a low thermal conductivity. Then, the HTC material is filled in the system, and the optimization objective is to find the HTC material distributions that can minimize the system's temperature at a given filling rate φ. The ratio of the thermal conductivity of the filled material to the substrate material is set to $k_f/k_s = 500$, which is large enough to make the results clear and intuitive. According to the kinetic theory, the relation between the phonon MFP l and thermal conductivity is $k = \frac{1}{3} C v_g l$, where C is the specific heat capacity and v_g is the phonon group velocity. The phonon MFP of the substrate material is selected as 250 nm in the calculation, but the selection of the absolute value will not affect the optimization process. The micro-nano-scale dimensions of t and w, along with the comparable MFP of phonons, result in prominent ballistic effect that enhances thermal spreading thermal resistance. To characterize the strength of the ballistic effect, two Knudsen numbers, Kn_t and Kn_w, are defined as $Kn_t = l_f/t$ and $Kn_w = l_f/w_g$, respectively, where l_f is the MFP of the filled material. For the current system, the relationship between Kn_w and Kn_t is fixed, with $Kn_w = 2.5Kn_t$. Therefore, in the subsequent analysis, Kn_t is used to represent the strength of the phonon ballistic effects in the system.

Verification by comparing with results under diffusive heat conduction

Previous research has compared the optimization results of the volume-to-point problem under diffusive heat conduction and ballistic-diffusive heat conduction, as depicted in Figure 3.[40] The Kn_{sub} and Kn_{fill} are the Knudsen number of substrate region and filled HTC material region, respectively. HTC materials exhibit branchless structures with larger characteristic sizes under ballistic-diffusive heat conduction due to the size effect of thermal conductivity, in contrast to the tree-like structures observed under diffusive

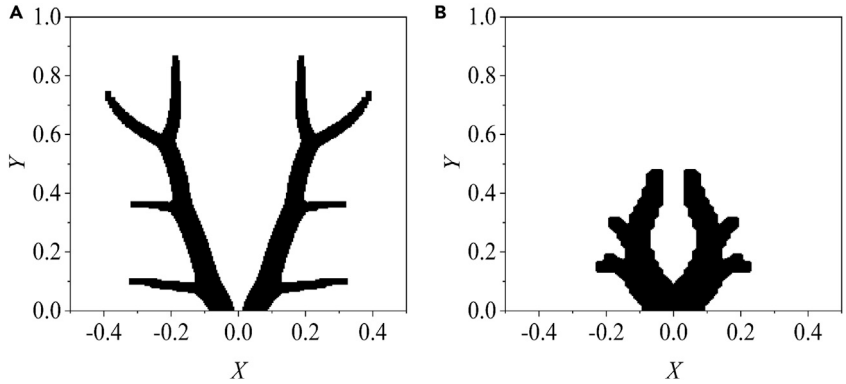

Figure 3. Topology optimization results of volume-to-point problem

(A) Diffusive heat conduction.

(B) Ballistic-diffusive heat conduction, $Kn_{sub} = 0.002$, $Kn_{fill} = 1$.

Table 1. The average dimensionless temperature ratio $T^*_{ave}/T^*_{ave,\ uni}$ of different material distributions at different Knudsen numbers

Kn_t	Uniform	Dist 1	Dist 2	Dist 3
0	100%	0.5%	1.4%	12.5%
5	100%	19.8%	10.6%	20.9%
125	100%	74.2%	60.9%	60.8%

Uniform distribution means that the material fills the design domain evenly in its initial proportions $\varphi = 0.01$. Dist 1, Dist 2, and Dist 3 are the optimized material distributions with Kn_t equal to 0, 5, and 125, respectively. The schematic diagram of different distributions is shown in Figures S2–S5.

heat conduction. However, achieving diffusive heat conduction and reducing the ballistic effect by adjusting the Knudsen number of the region can be challenging, especially when dealing with HTC ratios. Even at small Knudsen numbers for the substrate material, the ballistic effect of the HTC material region can still be significant. Moreover, reducing the thermal conductivity ratio may result in reduced optimization effects, with materials piling up at the low-temperature heat sink without effective optimization structures.[21] Therefore, in order to further validate the method, the optimization effects of different structures under various Knudsen numbers were compared.

Thermal simulations of different material distributions are performed with various Knudsen numbers, and the obtained T^*_{ave} is listed in Table 1. In the table, Dist 1, Dist 2, and Dist 3 are the optimized material distributions with Kn_t equal to 0, 5, and 125, respectively. The results of $Kn_t = 0$ are calculated under Fourier's heat conduction law. The T^*_{ave} of the uniform distributions is denoted by $T^*_{ave,\ uni}$, and $T^*_{ave}/T^*_{ave,\ uni}$ of different distributions is also calculated to evaluate the effectiveness of the material distributions.

As shown in Table 1, for a given Knudsen number, the lowest $T^*_{ave}/T^*_{ave,\ uni}$ occurs in the distribution optimized under the corresponding Knudsen number, which proves the validity of the developed optimization method. Moreover, for a given material distribution, $T^*_{ave}/T^*_{ave,\ uni}$ increases with the increase in Kn_t, indicating that the effectiveness of the filled HTC materials degrades with the enhancement of the phonon ballistic effect. $T^*_{ave}/T^*_{ave,\ uni}$ of the branch-shaped structure under Fourier's heat conduction law increases markedly as Kn_t increases, emphasizing the significant difference in the mechanism of ballistic-diffusive heat conduction compared to Fourier's heat conduction law. The results underscore the importance of taking phonon ballistic transport into account for heat dissipation optimization at the micro- or nano-scale. The following provides a detailed analysis of the reasons and mechanisms behind structural behavior at different Knudsen numbers.

Optimization results under different Knudsen numbers

Figure 4 depicts the optimized material distributions with different Knudsen numbers, where $X = x/w$, $Y = y/t$. Since the materials are only filled in the heat source region, the range of X for plotting is set as $[-0.02, 0.02]$. The system temperatures increase obviously with the increasing Knudsen number, the average T^* of optimized systems with $Kn_t = 0$, 5, and 125 are 0.023, 0.045, and 0.41, respectively. It indicates that the phonon ballistic effects can result in a significant increase in the thermal resistance and can diminish the effects of filled HTC materials. Besides the temperatures, the strength of phonon ballistic transport can have a marked impact on the optimal material distributions. As shown in Figure 4, for all conditions, the filled HTC materials form a contraction-expansion structure. Whereas when $Kn_t = 0$, there are branches in the optimized structure, which is similar to the optimization results of volume-to-point problem based on Fourier's heat conduction law.[18–20] As Kn_t increases, the proportion of branch-shaped structure declines, and the filled materials construct a whole piece of trunk structure. Also, with Kn_w increasing, the HTC materials are not directly placed in the heat source region. Instead, there is a distance between the filled materials and the heat source, and the distance increases with the increase of phonon ballistic effects. The two patterns, i.e. the branchless structure, and the gap between the filled materials and the heat source, can be attributed to the characteristics of ballistic-diffusive heat conduction. Since the contraction-expansion-shaped structure appears with different Knudsen number, it can be deduced that the shape can benefit heat extraction from the heat source and is caused by the characteristics of thermal spreading process. In the following of the paper, the different mechanisms are analyzed separately for better understanding of the optimization of hotspot systems in a ballistic-diffusive regime.

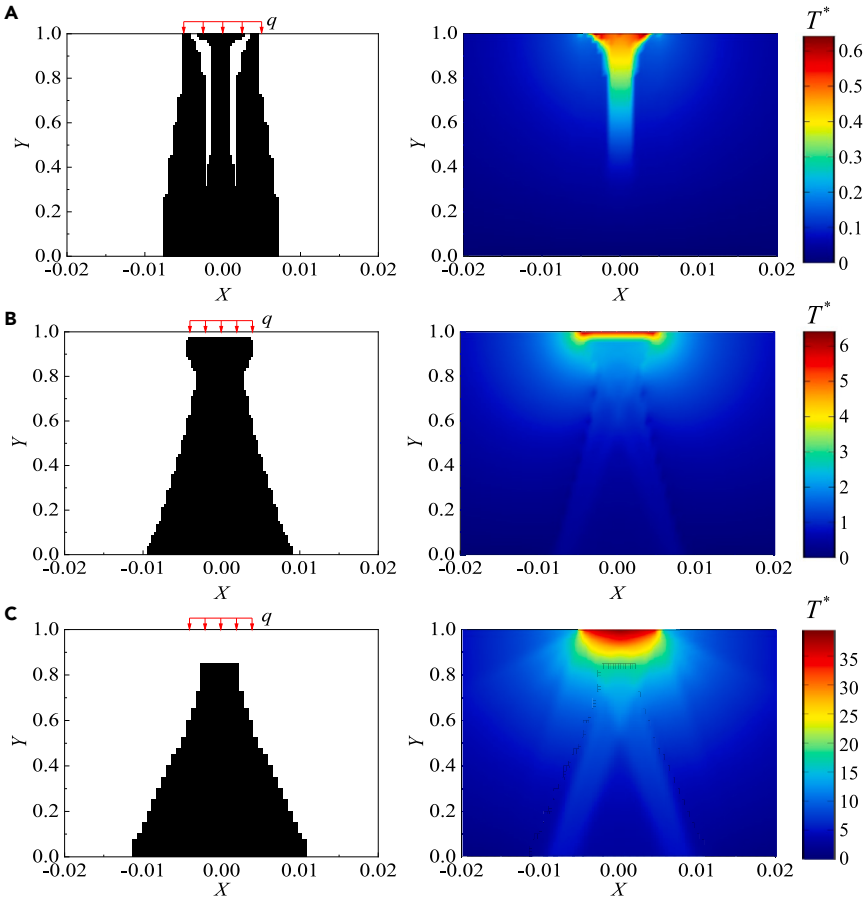

Figure 4. Optimized material distributions and temperature profiles varying with Kn_t and Kn_w

(A) Kn_t = 0 and Kn_w = 0.

(B) Kn_t = 5 and Kn_w = 12.5.

(C) Kn_t = 125 and Kn_w = 312.5.

Influence of thermal spreading

First, we will examine the influence of thermal spreading on the optimization results by considering cases where the Kn_t and the Kn_w are both set to zero, effectively ignoring the ballistic effect. Figure 5 compares the temperature profiles and heat flow distributions of the systems with uniform material distributions and optimized material distributions. It can be observed that for the case of uniform distributions, heat spreads from the hotspot, and the heat flow forms a semicircle around the heat source, resulting in significant thermal spreading resistance.[9] The highest T^* is 25, indicating that the total thermal resistance is 25 times as much as the 1-D thermal resistance. For the optimized structure, the filled HTC materials form a contraction-expansion-shaped heat conduction path between the heat source and the heat sink, transforming the thermal spreading process to nearly 1-D heat conduction, which can effectively reduce thermal spreading resistance.[41] In this case, the system temperatures drop significantly, with the highest T^* changing from 25 to 0.6 and the average T^* changing from 0.36 to 0.023. The results with higher Knudsen numbers also exhibit a similar tendency.

Influence of ballistic transport

To examine the influence of phonon ballistic transport on the optimization results, the temperature profiles and heat flow distributions with Kn_t = 5 and Kn_w = 12.5 are plotted in Figure 6. Similarly, with the heat conduction path formed by the filled materials, heat transport also changes from thermal spreading process to quasi 1-D heat conduction. However, the effectiveness of the formed heat conduction path is diminished since some phonons transport in a ballistic way.[36] Phonon ballistic transport occurs at two conditions,

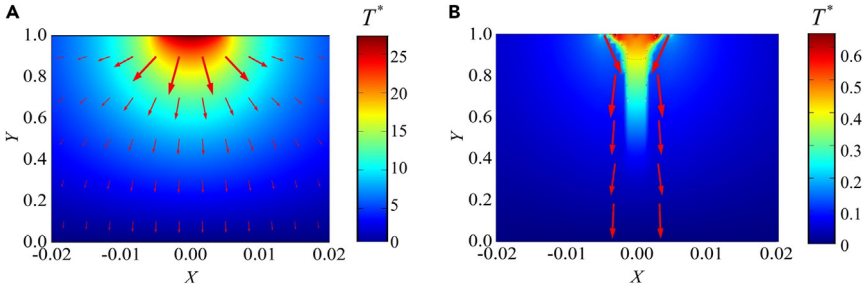

Figure 5. Temperature and heat flow distributions with $Kn_t = 0$ and $Kn_w = 0$
(A) uniform and (B) optimized material distributions.

i.e., when the phonon MFP is comparable with the structure size and the size of the heat source, respectively. The first one is the size effect related to the effective thermal conductivity of nanostructures which mainly depends on the Kn_t.[35–42] As the phonon MFP is comparable with the structure size, the effective thermal conductivity of the structure gets lower than its bulk value and decreases with its characteristic size decreasing. Therefore, although branch-shaped structures can help to transfer heat under diffusive heat conduction,[12] they can decrease the local effective thermal conductivity which deteriorates the heat dissipation. In this case, the optimized HTC material distributions tend to form a block of branchless structure.[40]

Another size effect occurs when the size of the heat source is comparable to the phonon MFP which mainly depends on Kn_w. The non-local phonon transport around the heat source can result in much higher local temperature compared to Fourier's heat conduction law-based predictions. Numerous experimental and numerical studies have been conducted to investigate the phenomenon.[35,43,44] During the material filling process in the optimization, although HTC material can facilitate heat conduction, its larger MFP can also lead to stronger phonon ballistic transport, increasing the local temperature. Therefore, there is a trade-off between the two opposite mechanisms during optimization. As a result, when the phonon ballistic effect is strong enough, a gap exists between the heat source and the filled HTC materials, and the gap increases as Kn_w increases due to the enhanced phonon ballistic effect. A comparative study is performed to verify the previously described discussion. Keeping the shape of the material distributions and the filling rate unchanged, the HTC materials are moved up to fill in the gap, as shown in Figure 7. For the modified structure, the highest T^* changes from 35 to 45, and the average T^* changes from 0.41 to 0.67. The results clearly illustrate the influence of heat source size-induced ballistic effect on optimization results in a ballistic-diffusive regime.

DISCUSSION

In this work, a new topology optimization method for ballistic-diffusive heat conduction is developed by combining the phonon BTE with SIMP method. With the utilization of the developed method, the optimization of HTC materials for efficient thermal spreading, a critical aspect for electronics, is examined

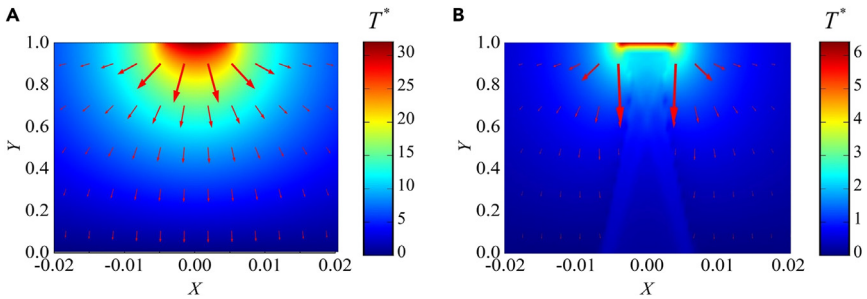

Figure 6. Temperature and heat flow distributions with $Kn_t = 5$ and $Kn_w = 12.5$
(A) uniform and (B) optimized material distributions.

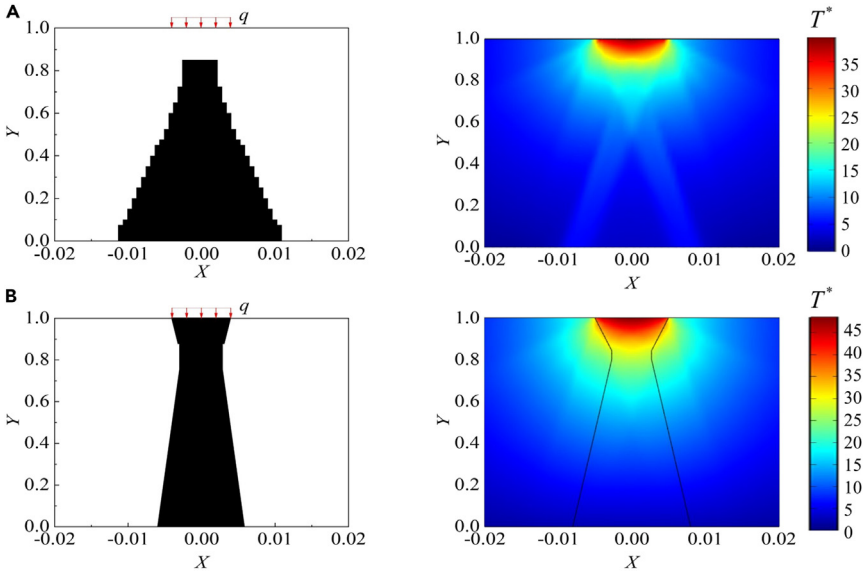

Figure 7. A comparative study of the influence of ballistic effect of heat source under Kn_w = 312.5
(A) the optimized distributions, (B) the modified distributions.

across different Knudsen numbers. It is found that the filled HTC materials form a contraction-expansion structure, which can transform the thermal spreading process around the heat source to quasi 1-D heat conduction, effectively reducing the thermal spreading resistance. Also, the optimization results indicate that phonon ballistic transport significantly affects the optimal material distributions. With the enhancement of phonon ballistic effects, the size effect makes the branch structure less effective and only trunk structures appear in the optimized distributions. Also, the ballistic effect with the heat source size comparable with phonon MFP can significantly increase the local temperature compared with Fourier's heat conduction law-based predictions. Thus, the HTC materials tend to be filled around the heat source with a gap instead of being filled directly in the heat source region in a ballistic-diffusive regime. The findings of the work can provide a more in-depth understanding of thermal spreading process in a ballistic-diffusive regime and the developed optimization method can be helpful for thermal management of advanced microelectronic chips.

Limitations of the study

At micro-nano scales, thermal resistance at material interfaces can lead to temperature jumps and impede heat transfer. The presence of HTC materials for heat dissipation can create thermal boundary resistance (TBR) at the filling-substrate interface, which can have a detrimental effect on optimization results. Incorporating TBR into the optimization process with SIMP requires further research. Moreover, practical devices like GaN HEMTs often contain heterostructures, which necessitate the development of optimization methods capable of handling multi-material and multi-hotspot systems.

STAR★METHODS

Detailed methods are provided in the online version of this paper and include the following:

- KEY RESOURCES TABLE
- RESOURCE AVAILABILITY
  - Lead contact
  - Materials availability
  - Data and code availability
- METHOD DETAILS
  - Phonon Boltzmann transport equation
  - Topology optimization

SUPPLEMENTAL INFORMATION

Supplemental information can be found online at https://doi.org/10.1016/j.isci.2023.107179.

ACKNOWLEDGMENTS

This work was supported by the National Natural Science Foundation of China (NNSFC) (Nos. 51825601, U20A20301 and 52250273).

AUTHOR CONTRIBUTIONS

Z.-L.T.: Formal analysis, Investigation, Writing-Original Draft. H.-L.L.: Conceptualization, Software, Methodology. Y.S.: Formal analysis, Writing-Original Draft. B.-Y.C.: Conceptualization, Supervision, Writing-review & editing.

DECLARATION OF INTERESTS

The authors declare no competing interests.

Received: April 17, 2023
Revised: May 15, 2023
Accepted: June 15, 2023
Published: June 23, 2023

REFERENCES

1. Chen, W.Y., Shi, X.L., Zou, J., and Chen, Z.G. (2022). Thermoelectric coolers for on-chip thermal management: materials, design, and optimization. Mater. Sci. Eng., R *151*, 100700. https://doi.org/10.1016/j.mser.2022.100700.

2. He, Z., Yan, Y., and Zhang, Z. (2021). Thermal management and temperature uniformity enhancement of electronic devices by micro heat sinks: a review. Energy *216*, 119223. https://doi.org/10.1016/j.energy.2020.119223.

3. Redmond, M., Manickaraj, K., Sullivan, O., Mukhopadhyay, S., and Kumar, S. (2013). Hotspot cooling in stacked chips using thermoelectric coolers. IEEE Trans. Compon. Packag. Manuf. Technol. *3*, 759–767. https://doi.org/10.1109/TCPMT.2012.2226721.

4. Cho, J., Li, Z., Asheghi, M., and Goodson, K.E. (2015). Near-junction thermal management: thermal conduction in gallium nitride composite substrates. Annual Rev. Heat Transfer *18*, 7–45. https://doi.org/10.1615/AnnualRevHeatTransfer.2015011335.

5. Nuttinck, S., Gebara, E., Laskar, J., and Harris, H.M. (2001). Study of self-heating effects, temperature-dependent modeling, and pulsed load-pull measurements on GaN HEMTs. IEEE Trans. Microw. Theor. Tech. *49*, 2413–2420. https://doi.org/10.1109/22.971629.

6. Mishra, U.K., Parikh, P., and Wu, Y.F. (2002). AlGaN/GaN HEMTs-an overview of device operation and applications. Proc. IEEE *90*, 1022–1031. https://doi.org/10.1109/JPROC.2002.1021567.

7. Razavi, M., Muzychka, Y.S., and Kocabiyik, S. (2016). Review of advances in thermal spreading resistance problems. J. Thermophys. Heat Trans. *30*, 863–879. https://doi.org/10.2514/1.T4801.

8. Ellison, G.N. (2003). Maximum thermal spreading resistance for rectangular sources and plates with nonunity aspect ratios. IEEE Trans. Comp. Packag. Technol. *26*, 439–454. https://doi.org/10.1109/TCAPT.2003.815088.

9. Hua, Y.C., Li, H.L., and Cao, B.Y. (2019). Thermal spreading resistance in ballistic-diffusive regime for GaN HEMTs. IEEE Trans. Electron Devices *66*, 3296–3301. https://doi.org/10.1109/TED.2019.2922221.

10. Salvi, S.S., and Jain, A. (2021). A review of recent research on heat transfer in three-dimensional integrated circuits (3-D ICs). IEEE Trans. Compon. Packag. Manuf. Technol. *11*, 802–821. https://doi.org/10.1109/TCPMT.2021.3064030.

11. Bejan, A. (1997). Constructal-theory network of conducting paths for cooling a heat generating volume. Int. J. Heat Mass Transf. *40*, 799–816. https://doi.org/10.1016/0017-9310(96)00175-5.

12. Song, M., Chen, K., and Zhang, X. (2021). Optimization of the volume-to-point heat conduction problem with automatic differentiation based approach. Int. J. Heat Mass Transf. *177*, 121552. https://doi.org/10.1016/j.ijheatmasstransfer.2021.121552.

13. Zhou, S., Chen, L., and Sun, F. (2007). Optimization of constructal economics for volume-to-point transport. Appl. Energy *84*, 505–511. https://doi.org/10.1016/j.apenergy.2006.09.005.

14. Tadjer, M.J., Anderson, T.J., Hobart, K.D., Feygelson, T.I., Caldwell, J.D., Eddy, C.R., Kub, F.J., Butler, J.E., Pate, B., and Melngailis, J. (2012). Reduced self-heating in AlGaN/GaN HEMTs using nanocrystalline diamond heat-spreading films. IEEE Electron. Device Lett. *33*, 23–25. https://doi.org/10.1109/LED.2011.2171031.

15. Volcheck, V.S., and Stempitsky, V.R. (2017). Suppression of the self-heating effect in GaN HEMT by few-layer graphene heat spreading elements. J. Phys, Conf. Ser. *917*, 082015. https://doi.org/10.1088/1742-6596/917/8/082015.

16. Dbouk, T. (2017). A review about the engineering design of optimal heat transfer systems using topology optimization. Appl. Therm. Eng. *112*, 841–854. https://doi.org/10.1016/j.applthermaleng.2016.10.134.

17. Xia, Z.Z., Cheng, X.G., Li, Z.X., and Guo, Z.Y. (2004). Bionic optimization of heat transport paths for heat conduction problems. J. Enh. Heat Transf. *11*, 119–132. https://doi.org/10.1615/JEnhHeatTransf.v11.i2.20.

18. Cheng, X., Xu, X., and Liang, X. (2009). Homogenization of temperature field and temperature gradient field. Sci. China Ser. E-Technol. Sci. *52*, 2937–2942. https://doi.org/10.1007/s11431-009-0244-8.

19. Chen, K., Wang, S., and Song, M. (2016). Optimization of heat source distribution for two-dimensional heat conduction using bionic method. Int. J. Heat Mass Transf. *93*, 108–117. https://doi.org/10.1016/j.ijheatmasstransfer.2015.09.041.

20. Marck, G., Nemer, M., Harion, J.L., Russeil, S., and Bougeard, D. (2012). Topology optimization using the SIMP method for multi-objective conductive problems. Numer. Heat Transfer, Part B *61* (6), 439–470. https://doi.org/10.1080/10407790.2012.687979.

21. Zhang, Y., and Liu, S. (2008). Design of conducting paths based on topology optimization. Heat Mass Tran. *44*, 1217–1227. https://doi.org/10.1007/s00231-007-0365-1.

22. Subramaniam, V., Dbouk, T., and Harion, J.L. (2018). Topology optimization of conductive

heat transfer devices: an experimental investigation. Appl. Therm. Eng. *131*, 390–411. https://doi.org/10.1016/j.applthermaleng.2017.12.026.

23. Sonmez, F.O. (2007). Shape optimization of 2D structures using simulated annealing. Comput. Methods Appl. Mech. Eng. *196*, 3279–3299. https://doi.org/10.1016/j.cma.2007.01.019.

24. Xu, X., Liang, X., and Ren, J. (2007). Optimization of heat conduction using combinatorial optimization algorithms. Int. J. Heat Mass Transf. *50*, 1675–1682. https://doi.org/10.1016/j.ijheatmasstransfer.2006.10.037.

25. Boichot, R., and Fan, Y. (2016). A genetic algorithm for topology optimization of area-to-point heat conduction problem. Int. J. Therm. Sci. *108*, 209–217. https://doi.org/10.1016/j.ijthermalsci.2016.05.015.

26. Hassani, B., and Hinton, E. (1998). A review of homogenization and topology optimization I—homogenization theory for media with periodic structure. Comput. Struct. *69*, 707–717. https://doi.org/10.1016/S0045-7949(98)00131-X.

27. Sigmund, O. (1994). Design of Material Structures Using Topology Optimization (Doctoral Dissertation, Technical University of Denmark).

28. Ziman, J.M. (2001). Electrons and Phonons: The Theory of Transport Phenomena in Solids (Oxford University Press).

29. Ju, Y.S., and Goodson, K.E. (1999). Phonon scattering in silicon films with thickness of order 100 nm. Appl. Phys. Lett. *74*, 3005–3007. https://doi.org/10.1063/1.123994.

30. Chen, L., Zhang, J., Lu, T., Cai, J., Zheng, J., Yao, J., Yi, S., Li, H., Chen, G., Zhao, H., et al. (2021). Non-Fourier phonon heat conduction at the microscale and nanoscale. Ann. Transl. Med. *9*, 555–569. https://doi.org/10.1038/s42254-021-00334-1.

31. Chen, G. (2001). Ballistic-diffusive heat-conduction equations. Phys. Rev. Lett. *86*, 2297–2300. https://doi.org/10.1103/PhysRevLett.86.2297.

32. Yang, R., Chen, G., Laroche, M., and Taur, Y. (2005). Simulation of nanoscale multidimensional transient heat conduction problems using ballistic-diffusive equations and phonon Boltzmann equation. J. Heat Transfer *127*, 298–306. https://doi.org/10.1115/1.1857941.

33. Hua, Y.C., and Cao, B.Y. (2014). Phonon ballistic-diffusive heat conduction in silicon nanofilms by Monte Carlo simulations. Int. J. Heat Mass Transf. *78*, 755–759. https://doi.org/10.1016/j.ijheatmasstransfer.2014.07.037.

34. Li, H.L., and Cao, B.Y. (2019). Radial ballistic-diffusive heat conduction in nanoscale. Nanoscale Microscale Thermophys. Eng. *23*, 10–24. https://doi.org/10.1080/15567265.2018.1520763.

35. Hua, Y.C., and Cao, B.Y. (2016). The effective thermal conductivity of ballistic–diffusive heat conduction in nanostructures with internal heat source. Int. J. Heat Mass Transf. *92*, 995–1003. https://doi.org/10.1016/j.ijheatmasstransfer.2015.09.068.

36. Hua, Y.C., and Cao, B.Y. (2016). Ballistic-diffusive heat conduction in multiply-constrained nanostructures. Int. J. Therm. Sci. *101*, 126–132. https://doi.org/10.1016/j.ijthermalsci.2015.10.037.

37. Danilchenko, B.A., Paszkiewicz, T., Wolski, S., Jeżowski, A., and Plackowski, T. (2006). Heat capacity and phonon mean free path of wurtzite GaN. Appl. Phys. Lett. *89*, 061901. https://doi.org/10.1063/1.2335373.

38. Evgrafov, A., Maute, K., Yang, R.G., and Dunn, M.L. (2009). Topology optimization for nano-scale heat transfer. Int. J. Numer. Methods Eng. *77*, 285–300. https://doi.org/10.1002/nme.2413.

39. Okamoto, N., Ohki, T., Masuda, S., Kanamura, M., Inoue, Y., Makiyama, K., Imanishi, K., Shigematsu, H., Kikkawa, T., Joshin, K., and Hara, N. (2009). SiC backside via-hole process for GaN HEMT MMICs using high etch rate ICP etching. CS MANTECH Conf. Dig. *1*, 7.

40. Li, H.L., and Cao, B.Y. (2019). Topology optimization of the volume-to-point heat conduction problem at micro-and nano-scale. Acta Phys. Sin. *68*, 200201. https://doi.org/10.7498/aps.68.20190923.

41. Chen, Y.S., Chien, K.H., Wang, C.C., Hung, T.C., Ferng, Y.M., and Pei, B.S. (2007). Investigations of the thermal spreading effects of rectangular conduction plates and vapor chamber. J. Electron. Packag. *129*, 348–355. https://doi.org/10.1115/1.2753970.

42. Dong, Y., Cao, B.Y., and Guo, Z.Y. (2014). Size dependent thermal conductivity of Si nanosystems based on phonon gas dynamics. Phys. E *56*, 256–262. https://doi.org/10.1016/j.physe.2013.10.006.

43. Vermeersch, B., Carrete, J., Mingo, N., and Shakouri, A. (2015). Superdiffusive heat conduction in semiconductor alloys. I. Theoretical foundations. Phys. Rev. B *91*, 085202. https://doi.org/10.1103/PhysRevB.91.085202.

44. Nghiem, T.T., Trannoy, N., and Randrianalisoa, J. (2019). Monte Carlo prediction of ballistic effect on phonon transport in silicon in the presence of small localized heat source. Nanotechnol *30*, 415403. https://doi.org/10.1088/1361-6528/ab2c1c.

45. Chen, G. (2005). Nanoscale Energy Transport and Conversion: A Parallel Treatment of Electrons, Molecules, Phonons, and Photons (Oxford University Press).

46. Cuevas, J.C., and García-Vidal, F.J. (2018). Radiative heat transfer. ACS Photonics *5*, 3896–3915. https://doi.org/10.1021/acsphotonics.8b01031.

47. Murthy, J.Y., and Mathur, S.R. (2002). Computation of sub-micron thermal transport using an unstructured finite volume method. J. Heat Transfer *124*, 1176–1181. https://doi.org/10.1115/1.1518495.

48. Narumanchi, S.V.J., Murthy, J.Y., and Amon, C.H. (2003). Simulation of unsteady small heat source effects in sub-micron heat conduction. J. Heat Transfer *125*, 896–903. https://doi.org/10.1115/1.1603774.

49. Hamian, S., Yamada, T., Faghri, M., and Park, K. (2015). Finite element analysis of transient ballistic–diffusive phonon heat transport in two-dimensional domains. Int. J. Heat Mass Transf. *80*, 781–788. https://doi.org/10.1016/j.ijheatmasstransfer.2014.09.073.

50. Majumdar, A. (1993). Microscale heat conduction in dielectric thin films. J. Heat Transfer *115*, 7–16. https://doi.org/10.1115/1.2910673.

51. Bao, H., Chen, J., Gu, X., and Cao, B. (2018). A review of simulation methods in micro/nanoscale heat conduction. ES Energy Environ. *1*, 16–55. https://doi.org/10.30919/esee8c149.

52. Sobolev, S.L. (2018). Hyperbolic heat conduction, effective temperature, and third law for nonequilibrium systems with heat flux. Phys. Rev. E *97*, 022122. https://doi.org/10.1103/PhysRevE.97.022122.

53. Sigmund, O., and Maute, K. (2013). Topology optimization approaches: a comparative review. Struct. Multidisc. Optim. *48*, 1031–1055. https://doi.org/10.1007/s00158-013-0978-6.

54. Sigmund, O., and Bondsgc, M.P. (2003). Topology Optimization. State-Of-The-Art and Future Perspectives (Technical University of Denmark (DTU)).

55. Bendsoe, M.P., and Sigmund, O. (2003). Topology Optimization: Theory, Methods, and Applications (Springer Science and Business Media).

56. Tcherniak, D. (2002). Topology optimization of resonating structures using SIMP method. Int. J. Numer. Methods Eng. *54*, 1605–1622. https://doi.org/10.1002/nme.484.

57. Sigmund, O., and Petersson, J. (1998). Numerical instabilities in topology optimization: a survey on procedures dealing with checkerboards, mesh-dependencies and local minima. Struct. Optim. *16*, 68–75. https://doi.org/10.1007/BF01214002.

58. Svanberg, K. (1987). The method of moving asymptotes—a new method for structural optimization. Int. J. Numer. Methods Eng. *24*, 359–373. https://doi.org/10.1002/nme.1620240207.

STAR★METHODS

KEY RESOURCES TABLE

REAGENT or RESOURCE	SOURCE	IDENTIFIER
Software and algorithms		
Thermal Modeling	COMSOL Multiphysics Software	RRID:SCR_014767
Graph Plotting	Origin Lab	RRID:SCR_014212

RESOURCE AVAILABILITY

Lead contact

Further information and requests for resources should be directed to and will be fulfilled by the lead contact, Bing-Yang Cao (caoby@tsinghua.edu.cn).

Materials availability

This study did not generate new unique reagents.

Data and code availability

- All data reported in this paper will be shared by the lead contact upon request.
- This paper does not report original code.
- Any additional information required to reanalyze the data reported in this paper is available form the lead contact upon request.

METHOD DETAILS

Phonon Boltzmann transport equation

At micro- and nano-scale, heat conduction is controlled by the phonon BTE. The steady-state phonon BTE under single-mode relaxation time approximation can be expressed as:

$$\vec{v}_g \cdot \nabla f = \frac{f_0 - f}{\tau} \quad \text{(Equation 1)}$$

where $\vec{v}_g$ is the group velocity, f is the phonon distribution function, f_0 is the equilibrium Bose-Einstein distribution, and τ is the relaxation time.[45] In this paper, the discrete ordinate method (DOM) is adopted to solve the phonon BTE. This method was originally used to solve the thermal radiation transfer equation and has also been proven to be a high-precision approach for the numerical solution of the phonon BTE.[46–49] The whole computational domain is discretized into a 40 × 1600 grids, which ensures adequate spatial resolution. In DOM, in analogy to photons, the phonon radiation intensity is defined by summing the contributions of phonons with different phonon branches:

$$I = v_g f \hbar \omega D(\omega) d\omega \quad \text{(Equation 2)}$$

where ω and $D(\omega)$ are the angular frequency and phonon density of states, respectively. Then, the phonon BTE can be rewritten in the form of equation of phonon radiative transfer (EPRT):

$$\vec{s} \cdot \nabla I = \kappa (I_0 - I) \quad \text{(Equation 3)}$$

where $\vec{s}$ is the unit direction vector, $I_0 = v_g f_0 \hbar w D(w) dw$ is the equilibrium phonon radiation density, and $\kappa = 1/l$ is the extinction coefficient, which is the inverse of the MFP.[50] For numerical solving in DOM, the solid angle space is discretized into N control angles, and the equation becomes:

$$\vec{s}_i \cdot \nabla I_i = \kappa (I_0 - I_i), i = 1, \ldots, N \quad \text{(Equation 4)}$$

where $\vec{s}_i$ is the unit direction vector, and I_i is the phonon radiation density in i-th solid angle .[51] The energy conservation equation can be expressed as:

$$\kappa \left(\sum_{i=1}^{N} w_i I_i - 4\pi I_0 \right) + \dot{q}_s = 0 \quad \text{(Equation 5)}$$

where w_i is the weight factor for the i-th solid angle, and $\dot{q}_s$ is the heat source per unit volume. By simultaneously solving the EPRT and energy conservation equation, the local phonon radiation density and temperature can be obtained. In this paper, the local temperature is calculated based on the equivalent phonon radiation intensity,[52] that is:

$$4\sigma_{phonon}T^4 = \sum_{i=1}^{N} w_i I_i \quad \text{(Equation 6)}$$

where σ_{phonon} is the phonon Stefan-Boltzmann constant. The dimensionless temperature T^* is introduced to eliminate the influence of the absolute value of parameters. By calculating the ratio of thermal spreading thermal resistance and the thermal resistance of one-dimensional heat conduction,[9] T^* is defined as:

$$T^* = \frac{(T - T_0)wk_s}{qw_g t} \quad \text{(Equation 7)}$$

Topology optimization

By using the DOM to calculate the system temperatures, topology optimization can be initiated to optimize HTC material distributions. The core idea of topology optimization is transforming design variables from discrete to continuous, allowing for the direct use of optimization methods for continuous variables.[27,53,54] Among the different transformation techniques, SIMP is an effective approach widely used in topology optimizations. SIMP sets the discrete design variable as a power function with respect to continuous relative density ρ which ranges from 0 to 1.[55,56] For thermal optimizations based on phonon BTE, the corresponding design variable is the extinction coefficient. Therefore, the extinction coefficient of any point in the domain can be expressed as:

$$\kappa = \kappa_s + (\kappa_f - \kappa_s)\rho^P \quad \text{(Equation 8)}$$

where κ_s and κ_f are the extinction coefficients of the substrate material and the filled material, respectively. The parameter p is the penalty coefficient used to penalize intermediate density values between 0 and 1 in the optimization to make ρ closer to the endpoint values, i.e., 0 or 1. In this work, p is set to 3.[53] To improve the numerical stability of the optimization, an explicit constraint on the global gradient of ρ is also employed in the objective function to limit the change of ρ.[57] The optimization problem can be written in mathematical form as:

$$\begin{aligned}
&\min_{0 \le \rho \le 1} : g = (1 - \alpha)\frac{T_{ave}}{T_{ave,ref}} + \alpha\frac{\int (\nabla\rho)^2 dA}{A} \\
&s.t. : s_i \cdot \nabla I_i = \kappa(I_0 - I_i), i = 1, \ldots, N \\
&\kappa\left(\sum_{i=1}^{N} w_i I_i - 4\pi I_0\right) + \dot{q}_s = 0 \\
&4\sigma_{phonon}T^4 = \sum_{i=1}^{N} w_i I_i \\
&\kappa = \kappa_s + (\kappa_f - \kappa_s)\rho^P \\
&\int \rho dA \le \varphi A
\end{aligned} \quad \text{(Equation 9)}$$

where T_{ave} is the average temperature of the system, $T_{ave,\ ref}$ is the preset reference temperature, α is the weight of the global gradient of ρ, A is the area of the design domain, and $\nabla\rho$ is the dimensionless global gradient of ρ. In the optimization, α is set as 0.001, which is beneficial to reduce the transition area but does not affect the optimization results.[40] The optimization process for Equation 9 is shown in Figure S1. The main procedures include: (1) initialization: discretize the design domain and set initial values for ρ; (2) system reanalysis: calculate the κ distributions using the SIMP method, solve the phonon BTE, obtain the temperature fields and objective function; (3) sensitivity analysis: calculate the derivatives of the objective function and the constraint function with respect to the design variable; (4) design update: according to the derivatives, determine the step size and update the design variable under constrain conditions; (5) judgment of convergence: when the convergence condition is satisfied, finish the iteration, otherwise repeat steps (2) – (4). In the optimization procedures, the sensitivity analysis is carried out using adjoin method, and the design update is realized by moving asymptotes method.[58] The convergence criterion

is set as $|\rho_j/\rho_{j-1}| \leq 0.001$, where j and $j-1$ represent the current iteration step and the last step, respectively. The filling rate φ is set as $\varphi = 0.01$, and the initial value for ρ is set equal to φ, i.e., the HTC materials are uniformly distributed in the system. Such a choice of φ ensures that the optimization produces efficient structures.[21] The topology optimization module and radiation in participating media module, available in the commercial software COMSOL, are utilized in this research. These modules enable to model the optimization process and the BTE separately, thereby facilitating the completion of the optimization calculations.